

DEPARTMENT OF PHYSICS AND ASTRONOMY
UNIVERSITY OF HEIDELBERG

Bachelor Thesis in Physics
submitted by

Jonathan Förste

born in Potsdam (Germany)

2015

THE AC-STARK SHIFT OF LITHIUM-6 IN A DIPOLE TRAP

This Bachelor Thesis has been carried out by Jonathan Förste at the
Physikalisches Institut Heidelberg
under the supervision of
Prof. Selim Jochim

ABSTRACT

This thesis investigates the AC-Stark shift in the ground and excited states of Lithium-6. The goal for our experiment is to implement spatially resolved fluorescence imaging of single atoms inside a microscopic dipole trap. To evaluate the feasibility, the trap depth for both the $2s_{1/2}$ -ground and the excited $2p_{3/2}$ -state is calculated using second order perturbation theory. The shift of resonance frequency of the optical transition for infrared light is predicted and measured using absorption imaging in our crossed dipole trap. The results are used to determine the potential depth of the microtrap. Both theory and experiment find that the Lithium-atom is also trapped in the excited state, but weaker than in the ground state. Therefore single site resolved imaging of individual atoms should be possible.

ZUSAMMENFASSUNG

Diese Arbeit untersucht den AC-Stark-Effekt in Grund- und angeregtem Zustand von Lithium-6. Ein Ziel unseres Experimentes ist es, einzelne Atome in einer mikroskopischen Dipolfalle mittels Fluoreszenz-Bildgebung räumlich aufzulösen. Um die entsprechende Realisierbarkeit zu bewerten werden die Fallentiefen für sowohl den $2s_{1/2}$ Grundzustand als auch den angeregten $2p_{3/2}$ -Zustand mittels Störungstheorie berechnet. Die Verschiebung der Resonanzfrequenz des entsprechenden optischen Übergangs wird theoretisch berechnet und in unserer optischen Dipolfalle mittels Absorptions-Bildgebung gemessen. Die Resultate werden benutzt um die Potentialtiefe der Mikrofalle zu bestimmen. Es stellt sich heraus, dass der angeregte Zustand in unerwartet weit rot verstimmten Dipolfalle ebenfalls gefangen bleibt, allerdings weniger stark als der Grundzustand. Das bedeutet, dass die räumliche Auflösung einzelner Atome möglich sein sollte.

CONTENTS

1. INTRODUCTION	9
2. THE EXPERIMENT	11
2.1. Preparing a Fermi gas	11
2.2. Imaging	12
2.2.1. Absorption imaging	12
2.2.2. Fluorescence imaging	13
3. THEORY	15
3.1. The Lithium Hamiltonian	15
3.2. Lithium level-structure	15
3.3. Magnetic field and Zeeman-splitting	17
3.4. Ac-stark shift	18
3.4.1. Lorentz oscillator model	18
3.4.2. Energy-shift in perturbation theory	19
3.5. Dipole traps	23
4. CALCULATION OF THE AC-STARK SHIFT	25
4.1. Polarizability of the lithium atom	25
4.1.1. Convergence for the calculation	28
4.2. Depth of the crossed dipole trap	29
4.3. Comparison to the classical formula	30
5. MEASUREMENT IN THE DIPOLE TRAP	31
5.1. Microtrap parameters	34
6. CONCLUSION AND OUTLOOK	35
A. APPENDIX	37
A.1. Potential of an induced dipole moment	37
A.2. Wigner 3-j and 6-j symbols	37
A.3. Wigner-Eckart theorem	38

1. INTRODUCTION

Many-body effects are of great interest for modern physics and many aspects of this field have vital importance not only for fundamental research, but for effects encountered and used in daily life. The behavior of electrons in a crystal for example is such a problem. It is the basis for many properties of condensed matter, such as the differences between metal, insulators and semiconductors. It is therefore of fundamental concern for all kinds of electronic applications. In several cases, the underlying laws of such processes can only be resolved when considering many-body systems. An example is superconductivity in cuprates, where the process is dominated by long-range electric and magnetic interaction [1]. Such systems cannot be calculated easily but require complex and time-consuming simulations, when treated numerically, since the complexity of such periodic quantum systems grows exponentially with size[2]. Studying the real systems in contrast, i.e. solid crystals or other materials, is similarly complicated, because solid materials limit the control over the parameters. Quantities such as density or depth of the atomic potentials cannot easily be changed in one material, which makes understanding the internal mechanisms much harder.

A promising field of research, that aims to overcome all these problems, is quantum simulation with ultracold gases. In the recent years many techniques have been invented to cool, trap and store neutral atoms, using devices like magneto optical traps or optical dipole traps[3], that allow methods like evaporative cooling to produce degenerate Fermi gases or Bose-Einstein condensates. By manipulating laser beams it has become possible to create potential landscapes, that emulate structures in solid crystals and allow to shape the Hamiltonian of such systems. They can be designed to resemble those, proposed in models of condensed matter physics and the respective parameters can be controlled with high precision [4]. One of the first experiments for example used interfering laser-beams that formed a standing wave. In this simulated lattice structure, loaded with a Bose-Einstein condensate, it was possible to see the phase transition from a superfluid to a Mott insulator[5].

Several techniques can be used to analyze the outcome of such experiments [6] such as resolving the occupation of individual lattice sites [7–10]. Latter method in particular provides unprecedented access to the state of quantum systems.

Our goal is to develop an imaging system with similar capabilities for our experiment. In this case, we trap Lithium-6 atoms in one or multiple optical tweezers (microtraps) [11]. Our plan is to briefly illuminate the trapped atoms resonantly and measure their fluorescence, that would give us the ability to count and spatially resolve the particles. Similar experiments already show this possibility for free falling and trapped atoms of different species [12, 13]. Before implementing this in our setup, we first have to determine how the AC-Stark shift due to the optical tweezers influences the ground and excited states of Lithium-6.

In this thesis this is calculated for the D₂-line and tested in experiment. The measurement is carried out in a bigger dipole trap, where the higher atom numbers allow spectroscopy by ap-

1. Introduction

plying absorption imaging. The shift of the resonance frequency is measured and compared to theory. It enables the prediction of trap depths for each state and allows conclusions regarding the imaging in the small optical tweezers.

The thesis starts by giving a general overview about the experiment with its features and goals. The next part shortly describes the theoretic foundation of the atomic structure followed by a detailed analysis of the interaction of particles with electromagnetic waves, leading to the formulas later used to calculate the AC-Stark shift for the $2s_{1/2}$ and $2p_{3/2}$ states of Lithium-6. After that the results of calculation and measurement of the predicted values are presented and evaluated.

2. THE EXPERIMENT

The key feature of the experiment is the possibility to prepare few atoms in a microscopic dipole trap with high fidelity. For this, we have to prepare a degenerate quantum gas of fermionic Lithium-6 atoms. A brief summary of our apparatus and the preparation scheme is given in this chapter. A more detailed description can be found in [14].

2.1. PREPARING A FERMI GAS

After vaporizing Lithium in an oven at 356 °C, the first component of the experiment is the Zeeman slower, that slows down the atomic beam with a resonant counterpropagating laser beam before it can be trapped inside the MOT. The slower is essentially a large tube behind the oven shutter (see figure 2.1), surrounded by coils. A strong laser beam is pointing along the slower in the opposite direction of the flying atoms. When being in resonance with an atomic transition, the photons get absorbed and the atoms are pushed in the direction of the laser. Because spontaneous emission is directed in random directions, this leads to slowing of the cloud. During their deceleration, the transition frequency of the atoms is Doppler-shifted with respect to the laser beam. Therefore a spatially varying magnetic field shifts the atoms back into resonance by use of the Zeeman effect.

After leaving the Zeeman slower, the atoms are captured in a magneto-optical trap (MOT). It consists of six counter-propagating near-resonant laser beams. The usage of many retro-reflected beams in different directions makes it possible not only to force the atoms in a certain direction, but to also affect all particles with a high absolute velocity. This reduces the overall average-speed and therefore cools the gas. However, since the force of the laser beams alone is only velocity-dependent, slow particles would exit the center of the crossed beams over time. For this reason a magneto-optical trap uses a magnetic quadrupole-field, that has zero strength in the middle and increases when moving further away from the center. The Zeeman-effect shifts the level-distance for the out moving atoms towards the frequency of the laser, which will then apply a force, dependent on the spatial position, enabling not only cooling but trapping and compression of the gas-sample. The natural linewidth of the used transition limits the cooling of the MOT to a temperature of around $140\mu\text{K}$. The system used in this experiment can store around 10^8 atoms.

However, to obtain a degenerate Fermi gas, the temperature has to be reduced much further. The next step on this ladder is to transfer the atoms from the MOT into the crossed dipole trap. It uses the laser beam of a 200 w Ytterbium fiber-laser (IPG YLR-200-LP) that is far red-detuned from the atomic transitions at 1070 nm. The beam's focus lies within the MOT, with a waist of approximately $40\ \mu\text{m}$ [15] (see figure 2.2). The beam is retro-reflected after leaving the vacuum chamber, forming the crossed shape of the dipole trap. To trap as many atoms as possible, the laser is ramped-up to full power, generating a trap depth of more than 3 mK. To further cool

2. The experiment

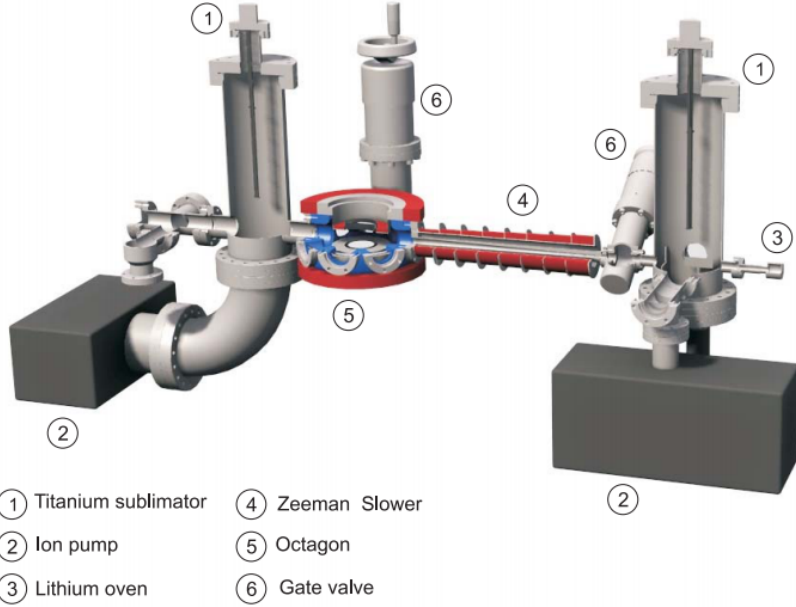


Figure 2.1.: Model of the experiments core-components. On the left the octagon-shaped vacuum chamber is visible, in which the experiment is carried out. Through the view ports lasers for the MOT and dipole-trap enter the chamber, (see figure 2.2). It is surrounded by coils providing magnetic field for several stages of the process. On the right one can see the oven and the Zeeman-slower connecting both parts.

the sample, the power is slowly ramped down, so the hottest atoms escape the potential and the rest of the cloud thermalizes at a lower temperature. This procedure is called evaporative cooling [3].

A small, tightly focused infrared laser-beam at 1064 nm, that intersects the crossed dipole-trap then forms the microtrap (MEPHISTO S from Innolight). The small dimensions of the trap result in large spacing between the allowed vibrational levels. To control the atom number in the microtrap, a magnetic field gradient tilts the dipole-potential. That leads to the escape of all atoms above a certain level. It allows the preparation of 1 to 10 particles with fidelities of over 90% [16].

2.2. IMAGING

At different stages of the experiment, the atoms can be imaged by different methods. While absorption imaging is used for diagnostics, we rely on fluorescence imaging for our experiments.

2.2.1. ABSORPTION IMAGING

Absorption imaging is a common method to image clouds of atoms[6]. A resonant beam is pointed at the sample, and partly gets absorbed. The shadow is captured on the sensor of a

ccd-camera. It shows the density distribution along the cloud. In the classical regime, where the Fermi gas is not degenerate, a Gaussian can be fitted to this distribution to obtain the atom number. When the gas is degenerate and follows Fermi statistics, this no longer holds and the calculation gets more complicated. A detailed analysis can be found in [17].

In this setup we use a tunable, grating stabilized diode laser (Toptica DL-100). We take three different images. The first picture images the atom cloud. The next picture is taken when the atom cloud is released from the trap, and the cloud is no longer visible. This image only contains the excessive imaging light which can be subtracted from the initial image. To account for disturbances of the ambient light, a third picture is taken.

The absorption not only depends on the density but also on the scattering cross section. For resonant light, the absorption is higher and therefore we will use this technique later on to find the resonance frequency of the atoms and to determine the AC-Stark shift.

However, this method is not suitable for resolving single atoms, because it requires a high atomic density. One therefore has to rely on the more basic fluorescence imaging.

2.2.2. FLUORESCENCE IMAGING

Our current method of imaging single photons is using the MOT to recapture the atoms after releasing them from the deactivated microtrap [18]. The trapping light gets absorbed and the resulting fluorescence is caught on a ccd-camera. the amount of captured light is used to determine the atom number, which is possible with high fidelity. The current imaging setup needs long exposure times of about one second. Since all atoms are recaptured in the same MOT, no spatial resolution is possible.

The next step will be imaging the atoms inside the microtrap, to compensate the disadvantage of the current setup. Instead of a MOT the atoms are excited in a non-trapping optical molasse. A retro-reflected resonant laser beam intersects the dipole trap and the emitted photons are once again captured, in this setup using a high numerical aperture objective and an EMCCD-camera, that allows single photon sensitivity. By holding the atoms in the trap while imaging, the fluorescence not only allows counting the absolute number, but to see the position of the single particles.

2. The experiment

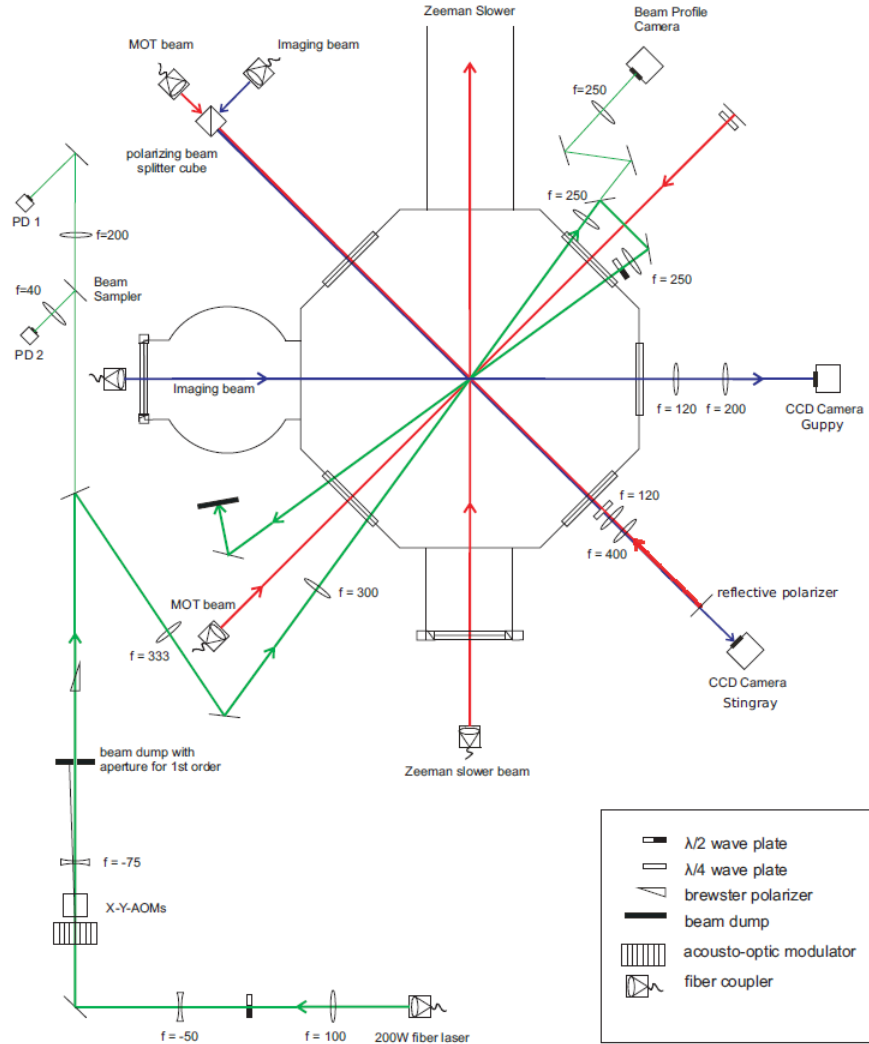


Figure 2.2.: Scheme of the laser set-up around the vacuum chamber [15]. The preparation of the Fermi gas uses two laser systems, consisting of the red resonant light for the MOT and the infrared laser of the dipole trap. A second resonant laser beam is used to do absorption imaging.

3. THEORY

To understand the function of an optical dipole-trap one has to understand how far detuned light, more specifically the electric field component, interacts with a neutral atom. There are several models providing different levels of accuracy for the respective application. The atom can be treated rather classically by regarding it as a harmonic oscillator driven by an electric field. It can be treated semi-classically by considering the quantum nature and structure of the atom while still approximate the incoming light as electromagnetic waves. In this model the problem can be solved in second-order perturbation theory. The third approach is treating the atom quantum mechanically as well as the light, now consisting of quantized photons interacting with the atom. For this thesis only the first two approaches were considered.

3.1. THE LITHIUM HAMILTONIAN

The problem of interaction between an atom, laser-light and in the case of this experiment also magnetic fields is represented by different parts in the total Hamiltonian. The basis for all calculations is the atomic Hamiltonian of Lithium-atoms H_A . The atom-light-interaction is represented by the Hamiltonian of the light itself H_L and the interaction Hamiltonian H_{AL} , that will lead to the AC-Stark shift. The last contribution is the magnetic field Hamiltonian H_M , that is resulting in the Zeeman effect.

$$H = H_A + H_L + H_{AL} + H_M \quad (1)$$

In our case H_L can be neglected and both H_{AL} and H_M will be considered perturbations of the atomic hamiltonian.

3.2. LITHIUM LEVEL-STRUCTURE

The atomic Hamiltonian H_A determines the energy eigenstates of the atomic species. In our experiment this is Lithium-6, a fermionic alkali-metal, whose electronic structure is mostly dependent of its single valence electron [19]. In this approximation, the *central-field approximation*, the two other bound electrons on innermost level only contribute to the central electric field, that is supposed to be spherically symmetric. Thus the calculation can follow the well understood model of hydrogen, that can be read in detail for example in [20]. The approach in this case considers an electron with the reduced mass μ in a Coulomb-potential.

$$U(\mathbf{r}) = -\frac{e^2 Z}{4\pi\epsilon_0 r} \quad (2)$$

3. Theory

That leads to the Hamiltonian:

$$H_A = \frac{p^2}{2\mu} - \frac{e^2 Z}{4\pi\epsilon_0 r} \quad (3)$$

Solving the Schrödinger-Equation considering this Hamiltonian leads to a set of wave-functions characterized by the quantum numbers N, L, m_L , N being the main quantum number, L the angular momentum quantum number and m_L the projection onto the coordinate axis. The energy-levels for different L are degenerate, but when the spin of the valence electron is considered this degeneracy is broken and the coupling of this spin to the orbital angular momentum leads to the fine-structure picture in which for Lithium $J = L \pm S$ and $m_J = J, J-1, \dots, -J+1, J$ are the respective quantum numbers. This leads to corrections, that have the form:

$$\Delta E_{FS} = E_n \left[\frac{Z^2 \alpha^2}{n} \left(\frac{1}{j+1/2} - \frac{3}{4n} \right) \right] \quad (4)$$

Where α stands for the fine-structure constant. The formula is composed of several corrections to the initial Hamiltonian. Nevertheless the real Lithium-atom has a substructure arising from

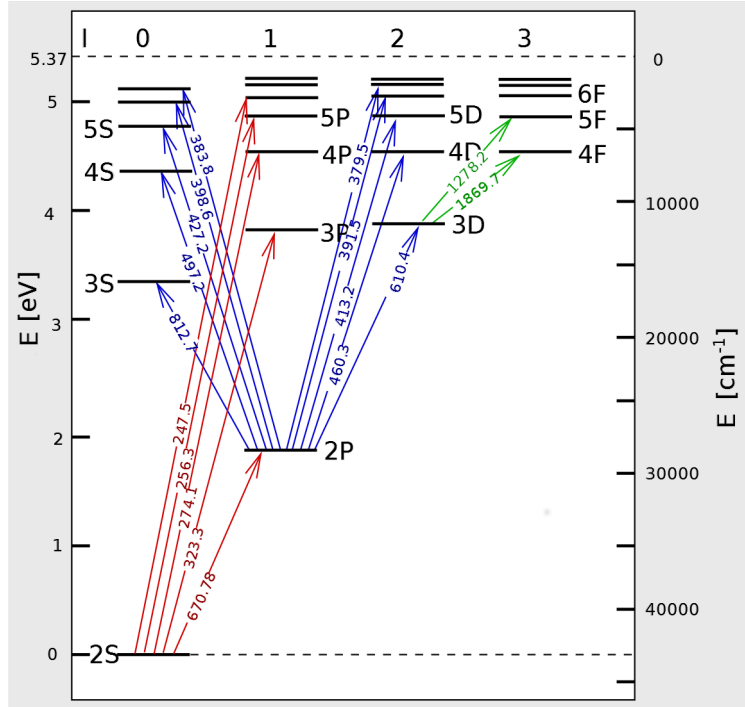


Figure 3.1.: Level structure of Lithium with the respective transitions, according to selection rules [21].

interaction of the nuclear spin and the valence electrons angular momentum. This effect results in the hyperfine structure that breaks the degeneracy of the levels with same quantum number J . In the picture of hyperfine structure the total angular momentum and the nuclear spin

3.3. Magnetic field and Zeeman-splitting

I couple to the new total angular momentum $F = J \pm I$ with their respective projections $m_F = F, F - 1, \dots, -F + 1, F$ that result in even finer splitting of the lines, which fully characterize the state of the Lithium-atom. The resulting corrections of the energy eigenvalues are of the form:

$$\Delta E_{HFS} = -\mu_I \cdot B_J \quad (5)$$

where μ_I is the magnetic moment of the nucleus and B_J is the magnetic field of the orbiting electron.

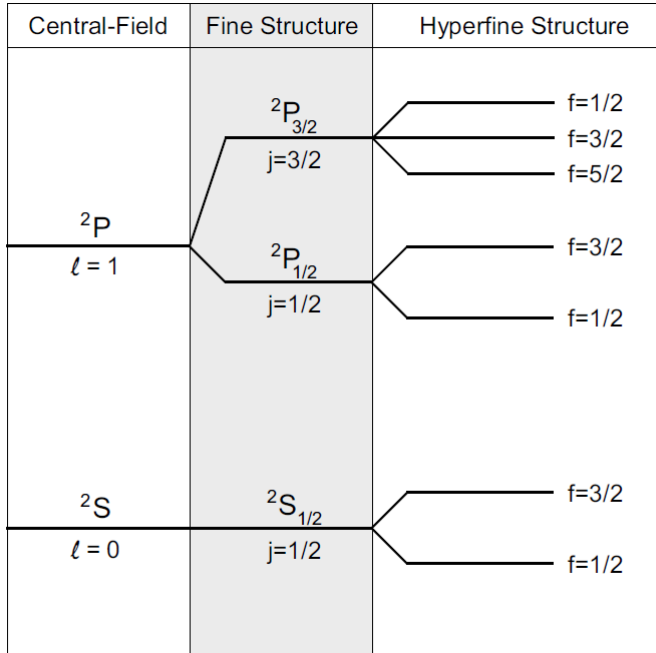


Figure 3.2.: Extract of the level structure for Lithium-6 in the fine and hyperfine regime [19]

3.3. MAGNETIC FIELD AND ZEEMAN-SPLITTING

Within the experiment, the atoms are exposed to strong magnetic fields. Therefore the Zeeman effect moves the respective levels, and therefore changes also the interaction with laser-light, i.e. the AC-Stark-Shift. In this approach we simply regard both effects as independent perturbations to the basic Hamiltonian. At strong magnetic fields, as used in the experiment, the Paschen-Back-Effect for hyperfine states dominates and instead of F and m_F , the quantum numbers J and m_J are still “good”. Therefore the formula for the shift of each state is given by:

$$\Delta E = g_J m_J \hbar \gamma B \quad (6)$$

With $\gamma = e/(2m_e)$ and g_J being the Landé-factor. The results are new values of energy-difference, i.e. detuning for the respective transitions. For Lithium-6 the effect shifts the levels in the order of 1 MHz/G.

3. Theory

3.4. AC-STARK SHIFT

The AC-Stark shift arises from the interaction of electric fields with the atom. Before treating this problem quantum-mechanically in terms of our Hamiltonian (1), we look at the problem in a classical model, that already results in a formula, that is very accurate in certain systems.

3.4.1. LORENTZ OSCILLATOR MODEL

Classically the problem of light-matter-interaction can be described in terms of an atomic dipole moment induced by an oscillating electric field, following [22]. The atom is hereby described as a damped harmonic oscillator driven by the field. Intuitively one can think of the electrons and the atomic nucleus being pulled away from each other by the electric force, resulting in an oscillation against each other. The potential arising from these conditions is the following. A detailed derivation of the potential can be studied in the appendix A.1.

$$U = -\frac{1}{2} \langle \mathbf{p}E \rangle \quad (7)$$

Here \mathbf{p} is the induced dipole moment, E the electric field. The time-average is introduced since the electric field in an electromagnetic wave is oscillating very fast and the atom “feels” an effective potential averaged over the oscillation. If we only consider the real part of $\mathbf{p}E \propto \cos^2$, the time average is $\langle \mathbf{p}E \rangle = 1/2 \operatorname{Re}(\alpha) E^2$. One can rewrite (7) in terms of the Intensity $I = 1/2 \epsilon_0 c E^2$:

$$U = -\frac{1}{2\epsilon_0 c} \operatorname{Re}(\alpha) I \quad (8)$$

To calculate the exact potential one has to obtain a value for the polarizability α . In this classical description an electron is considered bound to the core elastically with the oscillation Eigenfrequency ω_0 . This corresponds to the optical transition frequency. In our practical case that is the frequency of the Lithium-D2-line. In a real atom, there are of course multiple resonances, corresponding to multiple states of the electron, thus this approximation matches only certain cases in which the system can also be regarded as a quantum mechanical two-state-system. We will later see, that while this approach leads to a very accurate calculation for the Lithium ground state, it can not at all be applied to the calculation of the trapping potential for the first excited state.

The polarizability now can be calculated by solving the equation of motion of a driven and damped harmonic oscillator.

$$\ddot{x} + \Gamma_\omega \dot{x} + \omega_0^2 x = -\frac{eE(t)}{m_e} \quad (9)$$

for that the solution can be calculated using basic tools for solving ordinary differential equations. The result is then:

$$x(t) = -\frac{e}{m} \frac{1}{\omega_0^2 - \omega^2 - i\omega\Gamma_\omega} E e^{i\omega t} \quad (10)$$

Where the first part is defined as:

$$\alpha = \frac{e^2}{m_e} \frac{1}{\omega_0^2 - \omega^2 - i\omega\Gamma_\omega} \quad (11)$$

With

$$\Gamma_\omega = \frac{e^2\omega^2}{6\pi\epsilon_0 m_e c^3} \quad (12)$$

We can substitute $e^2/m_e = 6\pi\epsilon_0 c^3 \Gamma_\omega/\omega^2$ and define the on-resonance damping rate $\Gamma := (\omega_0/\omega)^2 \Gamma_\omega$ which results in the form:

$$\alpha = 6\pi\epsilon_0 c^3 \frac{\Gamma/\omega_0^2}{\omega_0^2 - \omega^2 - i(\omega^3/\omega_0^2)\Gamma} \quad (13)$$

We now can plug the real part of this expression in (7) and obtain the formula:

$$U_{dip}(\mathbf{r}) = -\frac{3\pi c^2}{2\omega_0^3} \left(\frac{\Gamma}{\omega_0 - \omega} + \frac{\Gamma}{\omega_0 + \omega} \right) I(\mathbf{r}) \quad (14)$$

In this case, the damping parameter Γ corresponds to the linewidth of the optical transition, which numerical value is $\Gamma=5.8724$ MHz for the considered D₂-line [19].

3.4.2. ENERGY-SHIFT IN PERTUBATION THEORY

After this classical treatment, we come back to calculating the same effect quantum mechanically. For calculating the energy-shift for the first excited state, this approach gets more trustworthy results since in contrast to the ground state of Lithium, it cannot be approximated by a two-level-system with only one transition. Therefore we have to solve the problem more precisely.

The interaction of the atom with laser-light is described by the two additional parts in the original Hamiltonian (1) $H_L + H_{AL}$. The light-Hamiltonian H_L is hereby negligible, because the regarded laser-light of the dipole-trap is far detuned from the relevant transition resonances and is seldomly absorbed by the atoms. Therefore, only the interaction Hamiltonian remains relevant, which depends on the dipole-operator \hat{p} and the electric-field-operator E and has the following form: $H_{AL} = -\hat{p}E = -erE$. It can be treated as a small perturbation of the atomic Hamiltonian, thus in the relevant second-order perturbation-theory the energy-shift is the following [22]:

$$\Delta W = \sum_{k \neq j} \frac{|\langle j | H_{AL} | k \rangle|^2}{W_k - W_j} \quad (15)$$

With j, k being all considered states of the atom and W_j, W_k the energy eigenvalues for these states of the initial Hamiltonian. Although the hyperfine splitting is highly relevant for the experiment itself, it is sufficient for the calculation of the Stark-Shift to only consider the fine-structure regime. Especially at strong fields, the hyperfine Paschen-Back effect is important. The different hyperfine states are close to degeneracy. The Hamiltonian still depends on the

3. Theory

product $J \cdot I$, but is considered as a small perturbation. The total angular momentum J therefore is a "good quantum-number" again. In the low-field regime the corrections due to hyperfine-splitting are small, because of the small energy differences compared to the relevant transitions between the levels in the fine-structure regime and the considered large detuning of the dipole-trap-light. Hence also there this picture is sufficient. In this case (15) can be expressed in terms of J and m_J and with the explicit form of H_{AL} this becomes[23]:

$$\Delta W_{Jm_j} = -e^2 \sum_{K \neq J} \sum_{m_k} \frac{\langle Jm_J | \mathbf{r}E | Km_K \rangle \langle Km_K | \mathbf{r}E | Jm_J \rangle}{W_K - W_J} \quad (16)$$

The main problem now is to calculate the coupling of different angular momenta. That is why most of the calculation is dedicated to simplify the calculation of all relevant Clebsch-Gordan coefficients.

We will now describe the electric field in terms of irreducible tensor operators:

$$E_{\pm} = \mp \frac{1}{2} \sqrt{2}(E_x \pm iE_y), \quad E_0 = E_z \quad (17)$$

$$r_{\pm} = \mp \frac{1}{2} \sqrt{2}(r_x \pm ir_y), \quad r_0 = r_z \quad (18)$$

(19)

In this notation we can rewrite (16) in terms of these operators:

$$\Delta W_{Jm_j} = -e^2 \sum_{K \neq J} \sum_{m_k} \sum_{\mu\nu} (-1)^{\mu+\nu} E_{\mu} E_{\nu} \frac{\langle Jm_J | r_{-\mu} | Km_K \rangle \langle Km_K | r_{-\nu} | Jm_J \rangle}{W_K - W_J} \quad (20)$$

With $\mu = 0, \pm 1$. Now, we define the following sum, that will be used later on. for simplification.

$$\mathcal{E}(L, m_L) := \sum_{\mu\nu} \sqrt{2L+1}(-1)^{m_L} \begin{pmatrix} 1 & 1 & L \\ \mu & \nu & -m_L \end{pmatrix} E_{\mu} E_{\nu} \quad (21)$$

We here also use the Wigner 3-j-symbol-notation, explained in appendix A.2. Using it, we can write the product in (20) in terms of this sum:

$$E_{\mu} E_{\nu} = \sum_{L=0}^2 \sum_{m_L=-L}^L \sqrt{2L+1}(-1)^{m_L} \begin{pmatrix} 1 & 1 & L \\ \mu & \nu & -m_L \end{pmatrix} \mathcal{E}(L, m_L) \quad (22)$$

For simplification, we can calculate (21) explicitly for different combinations of L and m_L .

$$\begin{aligned}
 \mathcal{E}(0,0) &= -\frac{1}{\sqrt{3}}(E_0^2 - 2E_{-1}E_1) = -\frac{1}{\sqrt{3}}(E_z^2 - 2(-\frac{1}{2}(E_x + iE_y)(E_x + iE_y))) \\
 &= -\frac{1}{\sqrt{3}}(E_z^2 + E_x^2 + E_y^2) = -\frac{1}{\sqrt{3}}E^2 \\
 \mathcal{E}(1,\pm 1) &= 0 \\
 \mathcal{E}(1,0) &= 0 \\
 \mathcal{E}(2,\pm 2) &= E_{\pm 1}^2 = \frac{1}{2}(E_x \pm iE_y)^2 \\
 \mathcal{E}(2,\pm 1) &= (E_x \pm iE_y)E_z \\
 \mathcal{E}(2,0) &= \sqrt{\frac{2}{3}}(E_0^2 + E_{-1}E_1) = \sqrt{\frac{2}{3}}(E_z^2 + \frac{1}{2}E_x^2 - \frac{1}{2}E_y^2 - \frac{1}{2}(E_x^2 + E_y^2)) \\
 &= \frac{1}{\sqrt{6}}(3E_z^2 - E^2)
 \end{aligned}$$

After finishing that horrible calculation, the next step is to evaluate the sum in (20), which is even more terrifying, as you can imagine!

The first step is to evaluate the inner part, that is the summation over the respective magnetic quantum numbers m_K . Thus we give it an own name and define:

$$\mathcal{S}(J, m_J) = \sum_{m_k} \sum_{\mu\nu} (-1)^{\mu+\nu} E_\mu E_\nu \langle Jm_J | r_{-\mu} | Km_K \rangle \langle Km_K | r_{-\nu} | Jm_J \rangle \quad (23)$$

The matrix elements can be calculated using the Wigner-Eckart theorem (See appendix A.3).

$$\begin{aligned}
 \mathcal{S}(J, m_J) &= (-1)^{J-K} |\langle J || r || K \rangle|^2 \times \\
 &\quad \sum_L \sqrt{2L+1} \sum_{m_L} \mathcal{E}(L, m_L) \sum_{\mu\nu} (-1)^{\mu+\nu} (-1)^{m_L} \begin{pmatrix} 1 & 1 & L \\ \mu & \nu & -m_L \end{pmatrix} \times \\
 &\quad \sum_{m_K} \left[(-1)^{J-m_J} \begin{pmatrix} J & 1 & K \\ -m_J & -\mu & m_K \end{pmatrix} (-1)^{K-m_K} \begin{pmatrix} K & 1 & J \\ -m_K & -\nu & m_J \end{pmatrix} \right] \quad (24)
 \end{aligned}$$

Note, that the first part of this term can be written in this way because using the Wigner-Eckart theorem the tensor operator in the matrix element now has become the normal spherical coordinate-operator in the respective reduced matrix element, which of course is hermitian. The sum over μ, ν and m_K can be evaluated and rewritten in terms of the 6-j symbol.

$$\begin{aligned}
 &\sum_{\mu\nu} (-1)^{\mu+\nu} (-1)^{m_L} \begin{pmatrix} 1 & 1 & L \\ \mu & \nu & -m_L \end{pmatrix} \times \\
 &\quad \sum_{m_K} \left[(-1)^{J-m_J} \begin{pmatrix} J & 1 & K \\ -m_J & -\mu & m_K \end{pmatrix} (-1)^{K-m_K} \begin{pmatrix} K & 1 & J \\ -m_K & -\nu & m_J \end{pmatrix} \right] \\
 &= (-1)^{2J} (-1)^{J-m_J} \begin{pmatrix} J & L & J \\ -m_J & 0 & m_J \end{pmatrix} \left\{ \begin{matrix} J & 1 & K \\ 1 & K & L \end{matrix} \right\} \delta_{m_L,0} \quad (25)
 \end{aligned}$$

3. Theory

This, together with the values for $\mathcal{E}(L, m_L)$, leads to the fact, that only terms with $L = 0, 2$ and $m_L = 0$ remain and the following holds:

$$\begin{aligned} \mathcal{S}(J, m_J) = & (-1)^{J-K} |\langle J || r || K \rangle|^2 \times \\ & \sum_L \mathcal{E}(L, 0) \sqrt{2L+1} (-1)^{J-m_J} \begin{pmatrix} J & L & J \\ -m_J & 0 & m_J \end{pmatrix} \begin{Bmatrix} J & 1 & K \\ 1 & K & L \end{Bmatrix} \end{aligned} \quad (26)$$

Now, we arrive at the point, where we can go back to evaluating (16). The finding in (26) means, that we can decompose ΔW_{Jm_J} into a sum over different L :

$$\Delta W_{Jm_J} = \sum_L \Delta W_{Jm_J}^L \quad (27)$$

in which each of the components can be written, using the form of (26).

$$\begin{aligned} \Delta W_{Jm_J}^L = & -e^2 \sum_{K \neq J} \frac{\langle J || r || K \rangle|^2}{W_K - W_J} \mathcal{E}(L, 0) \sqrt{2L+1} \\ & (-1)^{J+K} (-1)^{J-m_J} \begin{pmatrix} J & L & J \\ -m_J & 0 & m_J \end{pmatrix} \begin{Bmatrix} J & 1 & K \\ 1 & K & L \end{Bmatrix} \end{aligned} \quad (28)$$

For this equation we can analyze the only two different cases, namely for $L = 0, 2$. If we evaluate both components and use the values for $\mathcal{E}(0, 0)$ and $\mathcal{E}(2, 0)$, we get to both contributions to the energy-shift:

$$\Delta W_{Jm_J}^0 = -e^2 E^2 \frac{1}{3(2J+1)} \sum_{K \neq J} \frac{\langle J || r || K \rangle|^2}{W_K - W_J} \quad (29)$$

$$\begin{aligned} \Delta W_{Jm_J}^2 = & -e^2 (3E_z^2 - E^2) \sqrt{\frac{5J(2J-1)}{6(2J+3)(J+1)(2J+1)}} \times \\ & \frac{3m_J^2 - J(J+1)}{J(2J-1)} \sum_{K \neq J} (-1)^{J+K} \begin{Bmatrix} J & 1 & K \\ 1 & J & 2 \end{Bmatrix} \frac{\langle J || r || K \rangle|^2}{W_K - W_J} \end{aligned} \quad (30)$$

We now choose the electric field to be directed along the z-axis: $E = E\hat{z}$ so we can say, that $E_z^2 = E^2$. Thus follows:

$$\begin{aligned} \Delta W_{Jm_J}^2 = & -\frac{1}{2} e^2 E^2 4C \times \\ & \frac{3m_J^2 - J(J+1)}{J(2J-1)} \sum_{K \neq J} (-1)^{J+K} \begin{Bmatrix} J & 1 & K \\ 1 & J & 2 \end{Bmatrix} \frac{\langle J || r || K \rangle|^2}{W_K - W_J} \end{aligned} \quad (31)$$

We are hereby shortening $C := \sqrt{5J(2J-1)/6(2J+3)(J+1)(2J+1)}$. Note, that if the z-direction also defines the quantization axis in a magnetic field, this means assuming π -polarized laser-light. If the light is then supposed to be σ -polarized, the z-component has to be considered individually and it holds $E_z^2 = 1/2 E^2$. We now draw an analogy to the classical calculation

and link the total energy-shift to the induced dipole potential by defining a polarizability, composed of the now defined scalar and tensor polarizability. Note that a factor of $1/2$ is factored out in this sense.

$$\alpha := e^2 \left[\alpha_J^0 + \frac{3m_J^2 - J(J+1)}{J(2J-1)} \alpha_J^2 \right] \quad (32)$$

$$\alpha_J^0 = \frac{2}{3(2J+1)} \sum_{K \neq J} \frac{|\langle J || r || K \rangle|^2}{W_K - W_J} \quad (33)$$

$$\alpha_J^2 = 4C \sum_{K \neq J} (-1)^{J+K} \begin{Bmatrix} J & 1 & K \\ 1 & J & 2 \end{Bmatrix} \frac{|\langle J || r || K \rangle|^2}{W_K - W_J} \quad (34)$$

An additional factor has to be multiplied as in the classical formula. The electric field is oscillating and the average thus results in another factor of $1/2$, because we did not take the time into account, when calculating the polarizability.

$$U = -\frac{1}{2} \langle \alpha E^2 \rangle$$

$$U = -\frac{1}{4} e^2 \left[\alpha_J^0 + \frac{3m_J^2 - J(J+1)}{J(2J-1)} \alpha_J^2 \right] E^2 \quad (35)$$

3.5. DIPOLE TRAPS

The AC-Stark-Shift, as described above can, as stated in the beginning, be used to trap neutral atoms. We have seen so far (see 7, 35), that an electric field induces a dipole moment in the atom that leads to a dipole-potential. The resulting force is proportional to the gradient of the intensity-distribution around the atom, therefore to understand how a specific dipole trap works exactly, one has to study the properties of the applied laser beams.

Lasers normally emit Gaussian beams. The intensity distribution along the radial profile at a given point on the course of the beam is [22]:

$$I(r) = \frac{2P}{\pi w^2} \exp \left(-2 \frac{r^2}{w^2} \right) \quad (36)$$

With r being the radial coordinate, P the power of the beam and w the waist, that has the following value along the beam:

$$w(z) = w_0 \sqrt{1 + \left(\frac{z}{z_R} \right)^2} \quad (37)$$

with $z_R = \pi w_0^2 / \lambda$ being the so called Rayleigh range. In contrast to simple ray-optics, the focus of the Gaussian beam is not point-like but has a finite waist w_0 . At this point the intensity of the focused laser-beam is at its maximum:

$$I_{\max} = \frac{2P}{\pi w_0^2} \quad (38)$$

3. Theory

This determines the deepest point in the potential, independent of the exact geometry of the trap, in case the center has a Gaussian form. This is the case for both dipole-traps used in the experiment, that are described in the previous chapter.

4. CALCULATION OF THE AC-STARK SHIFT

The calculation of the Ac-Stark-Shift is performed, using the formulas resulting from perturbation theory in the previous sections. The first part of this chapter reviews the main results regarding the polarizabilities of the ground and first excited state. This will reveal also whether the excited state can also be trapped in the high intensity region of the lasers and how the trapping compares to that of the ground state. All calculations use the computer algebra system mathematica.

For the measurement, concrete shift calculations are made for the crossed dipole trap. At the end of next chapter, values for the microtrap will be presented, that will suggest, in how far the goal of imaging atoms in small traps and single sites can be managed. The magnetic field, and thus the quantization axis is defined to be along the z-direction.

4.1. POLARIZABILITY OF THE LITHIUM ATOM

For the calculation of the polarizabilities for the respective states, the geometry and power of the used laser-beams are not important. They only depend on the wavelength of the incoming light and on its polarization, which plays a notable role for the tensor-polarizability in the vicinity of a transition resonance. It renders unimportant, when using very far detuned trap-light. Before talking about concrete results, we recall the formulas given in the theory-section.

$$\alpha = \left[\alpha_J^0 + \frac{3m_J^2 - J(J+1)}{J(2J-1)} \alpha_J^2 \right] \quad (39)$$

$$\begin{aligned} \alpha_J^0 &= \frac{2}{3(2J+1)} \sum_{K \neq J} \frac{|\langle J || r || K \rangle|^2}{W_K - W_J} \\ \alpha_J^2 &= 4C \sum_{K \neq J} (-1)^{J+K} \begin{Bmatrix} J & 1 & K \\ 1 & J & 2 \end{Bmatrix} \frac{|\langle J || r || K \rangle|^2}{W_K - W_J} \end{aligned}$$

Following [24], the polarizability is calculated using atomic units (a.u.). For the calculation transitions up to $n = 7$ were considered. The respective dipole-transition matrix elements are listed below, together with the energy-differences between the levels.

4. Calculation of the ac-stark shift

Transition	Matrix-element [a.u.]	Resonance [nm]
$2s_{1/2} - 2p_{1/2}$	3.3169	670.791
$2s_{1/2} - 2p_{3/2}$	4.6909	670.776
$2s_{1/2} - 3p_{1/2}$	0.183	323.2657
$2s_{1/2} - 3p_{3/2}$	0.259	323.2657
$2s_{1/2} - 4p_{1/2}$	0.160	274.1203
$2s_{1/2} - 4p_{3/2}$	0.226	274.1203
$2s_{1/2} - 5p_{1/2}$	0.1198	256.2312
$2s_{1/2} - 5p_{3/2}$	0.169	256.2312
$2s_{1/2} - 6p_{1/2}$	0.0925	247.5061
$2s_{1/2} - 6p_{3/2}$	0.131	247.5061
$2s_{1/2} - 7p_{1/2}$	0.0737	242.5426
$2s_{1/2} - 7p_{3/2}$	0.1042	242.5426
$2p_{3/2} - 3s_{1/2}$	3.4403	812.645
$2p_{3/2} - 4s_{1/2}$	0.9167	497.175
$2p_{3/2} - 5s_{1/2}$	0.4929	427.313
$2p_{3/2} - 6s_{1/2}$	0.3268	398.554
$2p_{3/2} - 7s_{1/2}$	0.2397	383.564
$2p_{3/2} - 3d_{3/2}$	2.2658	610.366
$2p_{3/2} - 3d_{5/2}$	6.7975	610.364
$2p_{3/2} - 4d_{3/2}$	0.8627	460.283
$2p_{3/2} - 4d_{5/2}$	2.5882	460.289
$2p_{3/2} - 5d_{3/2}$	0.5015	413.262
$2p_{3/2} - 5d_{5/2}$	1.5045	413.262
$2p_{3/2} - 6d_{3/2}$	0.3435	391.535
$2p_{3/2} - 6d_{5/2}$	1.0306	391.535
$2p_{3/2} - 7d_{3/2}$	0.2565	379.507
$2p_{3/2} - 7d_{5/2}$	0.7696	379.507

Figure 4.1.: Reduced Dipole-Transition-Matrix-Elements [24] in a.u. and the respective detuning [25], i.e. the resonance-energy for the relevant levels: $1s_2 2s_{1/2}$ and $1s_2 2p_{3/2}$

Figure 4.2 shows how the polarizability behaves for different levels and different wavelengths of the incoming laser light. In this case, π -polarized light is assumed. The qualitative behavior does not change due to different polarizations, only the magnitude of the tensor polarizability. The differences in the practical case of our experiment will be discussed later on.

4.1. Polarizability of the lithium atom

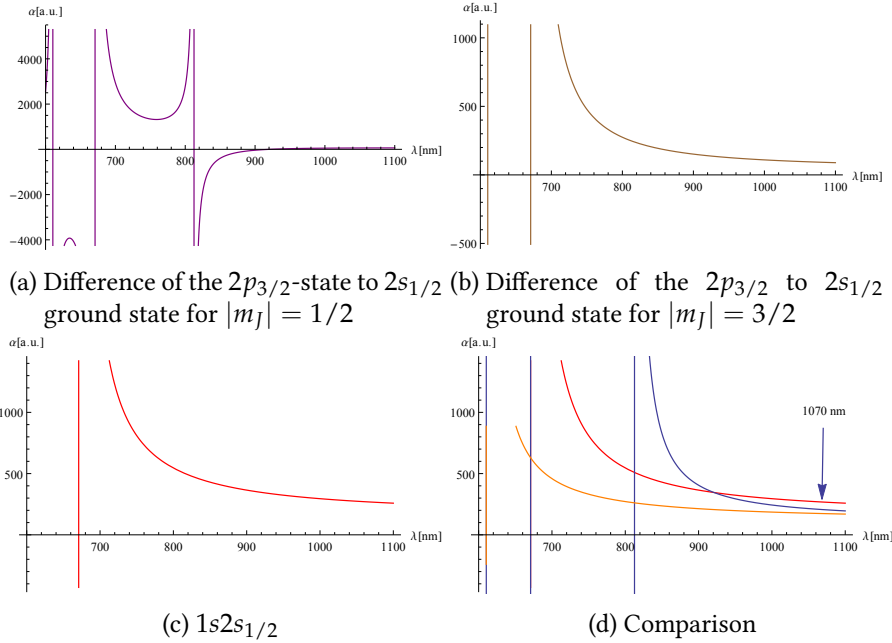


Figure 4.2.: Polarizability α for the states $1s2s_{1/2}$ (red), $1s2p_{3/2}$, $|m_j|=1/2$ (blue) and $1s2p_{3/2}$, $|m_j|=3/2$ (orange) and the difference between the ground and the two excited states (Purple, Brown). It is visible, that for high wavelengths, i.e. far detuning the differences between the states asymptotically tend towards relatively small values.

What can be seen in the plots are some interesting properties. The first important result is, that considering a far detuned light-source, the ground state as well as the excited state show positive polarizabilities. This fundamentally contradicts the picture of a two-level system, for example described in [26]. In this model, the excited state will be shifted in opposition to the ground state, i.e. the relative sign in the polarizability flips. This reflects the fact, that in a real atom, especially in the excited states of Lithium, the structure is much more complicated, than what results from the two-level approximation, because many different levels are roughly in the same energy-range and no single transition dominates (see figure 4.1). Practically this results in the fact, that both the ground-state and the first excited states can be trapped in a red-detuned dipole-trap, because the positive polarizability results in a negative potential. Therefore the atoms are attracted to the highest intensity of the laser-beam. The difference lies in the exact values. For far detuned light, the ground state shows a higher polarizability than both excited states, and therefore feels a deeper potential. From figure can be seen, how the different excited states behave relative to the ground state for the both relevant laser-wavelength for the crossed dipole-trap and microtrap in the experiment. The difference though can be considered negligible.

As stated in the theory-section, the magnetic field shifts the different levels, depending on their respective angular momentum and magnetic quantum numbers. This results in different values for the detuning, that determine the polarizability. However, at 527 G, that is a high field in the framework of the experiment, the shifts due to the Zeeman-effect are very small

4. Calculation of the ac-stark shift

and the overall change in the resonance is orders of magnitude below the error in predicting the differential light shift altogether. This is an important result, because the trapping efficiency therefore does not significantly change, when applying different magnetic fields, that are used to tune the atoms interaction strength.

State	α at 1070 nm [α_{ground}]	α at 1064 nm [α_{ground}]
$2p_{3/2}, m_j = 1/2$	0.7694	0.7726
$2p_{3/2}, m_j = 3/2$	0.6487	0.6472

Figure 4.3.: Polarizabilities of the excited states for the relevant laser-wavelengths, in relation to the ground state polarizability.

The picture looks different, when considering higher frequencies, especially when comparing the two excited states with different magnetic quantum number. Below around 900 nm and $m_J = 3/2$ the absolute value of the polarizability is much higher than for both other states. Mathematically this can easiest be seen, when looking at the formula for the total polarizability. The tensor-part of this formula is multiplied by a factor, that is -1 or +1, depending on whether $|m_J| = 1/2$ or $|m_J| = 3/2$. This means, that it decides whether the tensor part is added or subtracted, when calculating the total value. If it is subtracted, in case of $|m_J| = 3/2$, in the vicinity of many resonances, the diverging terms will cancel each other out and instead of a singularity a finite value is the result.

In the regime of far detuned light, all magnetic sublevels strive towards the same value of polarizability, only depending on the scalar part, that is isotropic and does not depend on the light-polarization.

4.1.1. CONVERGENCE FOR THE CALCULATION

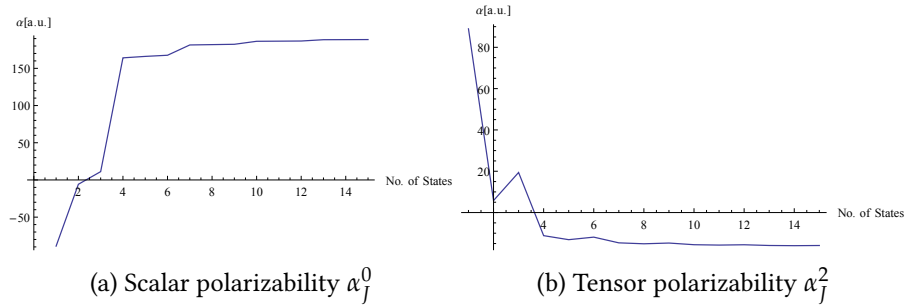


Figure 4.4.: Convergence of the polarizability value for the excited state $1s2p_{3/2}, |m_j| = 3/2$ at 1070 nm.

Another interesting question is, how far one has to go in calculating the energy shift in this perturbation framework to get a good approximation of the actual value. The maximum accu-

4.2. Depth of the crossed dipole trap

racy, as written above, was considering levels up to $n = 7$. Figure (4.4) shows how the value of α changes when considering higher levels. The x-coordinate is simply the index of the states, counted from low to high detuning. One can see, that for the excited state, when going above $n = 3$ the curve seems to converge. However for up to $n = 3$, the value of α reaches only 85% of its value at the full calculation. It reaches 95% not until considering levels up to $n=5$. This is because all levels further above show little differences in detuning and also in the respective reduced matrix elements and therefore the states contribute similarly to the final result. In the case of the ground state, considering only the two lowest transitions already results in a value that has 99.8% of the final value. Therefore the high precision calculation when taking into account higher levels brings little benefit.

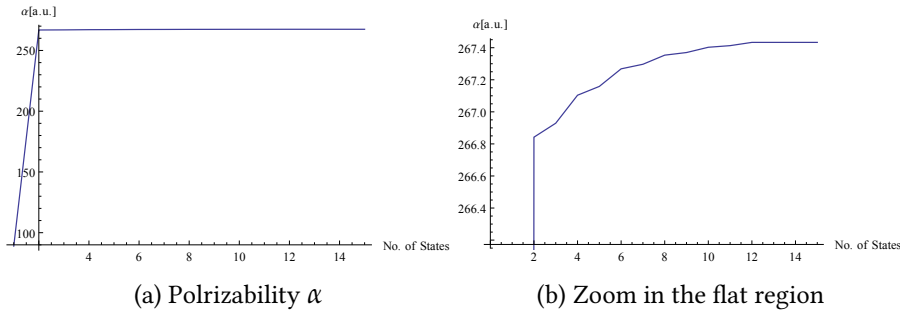


Figure 4.5.: Convergence of the polarizability value for the ground state $1s2s_{1/2}$ at 1070 nm.

4.2. DEPTH OF THE CROSSED DIPOLE TRAP

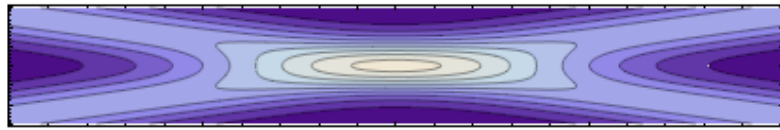


Figure 4.6.: Schematic intensity distribution for crossed dipole trap. The depth is decided by the maximum intensity in the center, that can be calculated considering a Gaussian profile.

We now want to calculate the trap depth and the differential light shift, that can be measured in the experiment. Since the ground state and the first excited states have different polarizabilities, also the relative light shift behaves differently. Therefore the resonance frequency, that depends on the energy-difference between the levels, shifts as well. Using absorption imaging, it can be measured with good precision. Determining the trap depth directly can be more complicated. Although the crossed dipole-trap is not a single beam, the beam profile in the middle, where the intensity is at its maximum, is Gaussian. That means, that like for a normal Gaussian beam,

4. Calculation of the ac-stark shift

the trap is characterized by its beam-power and waist (see 3.5). The power in this case is two times the power leaving the laser initially, since it gets reflected and forms the second beam as well. The waist in this case is $40 \mu\text{m}$, with an error estimated to be around 5%. The experiment will later be performed at multiple powers, that have a much higher accuracy with an error, being roughly 0.1%.

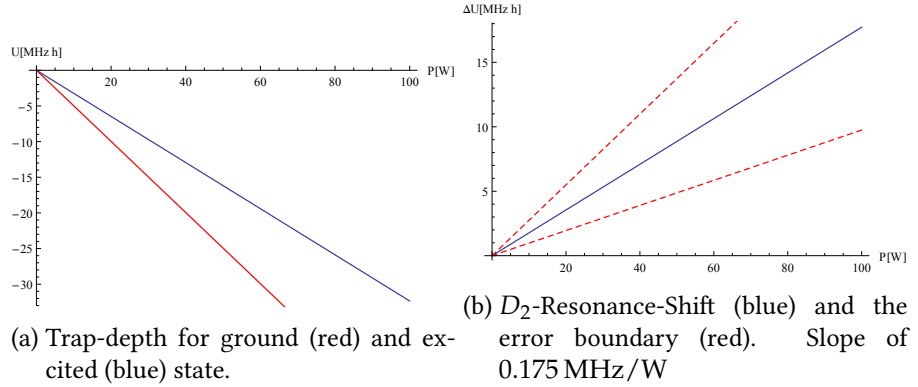


Figure 4.7.: Potential for ground ($2s$) and excited ($2p_{3/2}|m_J| = 3/2$) state and the difference of both, i.e. the shift of the D_2 -resonance, for different total powers of the trap-beam.

4.3. COMPARISON TO THE CLASSICAL FORMULA

Since the classical formula in (14) is widely used to calculate depths for optical dipole traps it is interesting to see, in how far it differs from the quantum-mechanical approach. For the excited state, it is not possible to calculate a good value using this approach. For the ground state however, for that the coupling to other states is dominated by the transition to the first excited state, the formula gives reasonable results. The values differ only 0.3% when calculating the shift considering transitions up to $n=7$ and using 1070 nm light. When only considering the D -Line transition, both values are the same in range and differ about 0.01 %. That shows, that using the approach of a harmonic oscillator to model the dipole-trap potential gives good results, when dealing with a system that can be approximated to only consist of two states. In the case of the Lithium-6 ground state, where for infrared light and higher excited states the transitions are very far detuned, the model gives a good estimate, that is less complicated to calculate than the approach of perturbation theory.

5. MEASUREMENT IN THE DIPOLE TRAP

For evaluating the calculations in the experiment the resonance-frequency of the D₂-Line was measured. The measurement of the ac-Stark shift is done in the crossed dipole-trap. The magnetic field however was at 527 G for every measurement. To find the resonance peak in the respective setting the atom number is measured using absorption imaging. The frequency of the imaging laser is hereby scanned over the considered resonance, taking 5 images for every step in detuning and taking the average. To find the differential light shift, the pictures are taken either with the activated dipole-trap or with the laser-beams turned off, leaving minimum time of flight in order to get reliable results. The used D_2 -line corresponds to the transition from $2s \rightarrow 2p_{3/2}$. For technical reasons only the incoming beam of the dipole trap is π -polarized and the reflected beam has components in σ^+ and σ^- -direction. This changes the value for the tensor-polarizability of the excited state but since the trap is far detuned, this component already plays a minor role and the different polarizations should change the overall differential shift only around 0.1 MHz, which cannot be resolved. The initial cloud is a mixture of two spin-species. However, due to the magnetic field the two ground states of $m_J = \pm 1/2$ differ by around 80 MHz due to the Zeeman-effect. Because of the polarization of the imaging laser all excited states would be shifted in the positive direction. While this does not change the behavior of the ac-Stark shift significantly, it does make sure, that only a transition from one ground state is resonant at once. In our case this was the transition: $m_J = +1/2 \rightarrow m_J = +3/2$. Since the excited state is expected to be shifted less than the ground state by the ac-Stark shift, the energy difference should increase, leading to a higher resonance frequency and a lower resonance wavelength. The shift is expected to be 0.175 ± 0.060 MHz/W and therefore the resonance frequency for 12.35 W should be 4.3 ± 1.5 MHz lower, when activating the dipoletrap. The resulting graph for this power can be seen in figure 5.1. To compare the behaviour as well as the exact values with the theory, different powers were measured and plotted in figure 5.2. As can be seen in figure 5.2 the shifts show a linear behaviour. The fit was fixed at ($P = 0, \Delta E_{\text{dif}} = 0$) and still shows a very good agreement with the prediction. The slope is 0.3274 ± 0.0013 MHz/W of initial beam-power. For a more general statement the value is also given in terms of the intensity:

$$\Delta E_{\text{dif}} / I = 0.4426 \pm 0.0028 \text{ MHz} \frac{1}{\text{mW}/\mu\text{m}^2} \quad (40)$$

Using this value, we also can calculate the trap depth, when knowing the relation of both polarizabilities for ground and excited states. The formula is derived using the fact, that the

5. Measurement in the dipole trap

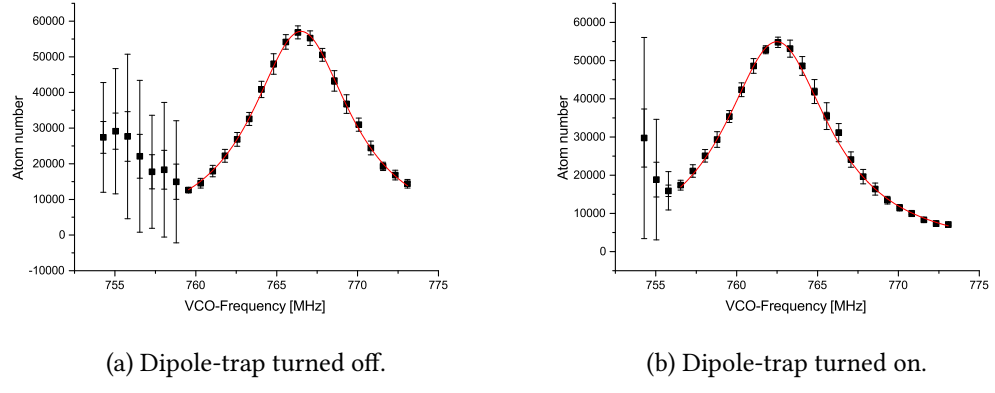


Figure 5.1.: Resonance peak for the transition: $2s \rightarrow 2p_{3/2}$, $m_J = +3/2$ at 1070 nm. The power at this measurement was 12.35 W. The scale shows frequencies of the voltage-controlled oscillator determining the detuning of the laser and is fixed arbitrarily. Also higher frequencies actually mean red detuning. It therefore shows only the relative shift. A Lorentzian function (red) was fitted to the values, whose parameters were used to determine the center position of the peak. In the range, where the laser was effectively off-resonance the seen atom-cloud lost its gaussian profile, and therefore no fit was possible to determine the atom number. This accounts for the high errors in this range.

relation between the polarizabilities and thus the light shifts is constant for every power.

$$U_g = - \frac{1}{1 - \alpha_e / \alpha_g} \cdot \Delta E_\delta \quad (41)$$

$$U_e = - \frac{1}{1 - \alpha_g/\alpha_e} \cdot \Delta E_\delta \quad (42)$$

In this case ΔE_δ stands for the relative shift of the levels relative to each other, i.e. the shift of the resonance. The results of the experiment translate into depths of the trap potential for the ground and excited state with the following values:

$$U_g/I = - (120.32 \pm 0.48) \mu\text{K} k_B \frac{1}{\text{mW}/\mu\text{m}^2} \quad (43)$$

$$U_e/I = - (78.05 \pm 0.31) \mu\text{K} k_B \frac{1}{\text{mW}/\mu\text{m}^2} \quad (44)$$

Also the measurement can make it possible to find values for other quantities of the trap. The waist of the trap beam for example is usually not easy to measure exactly, in contrast to its

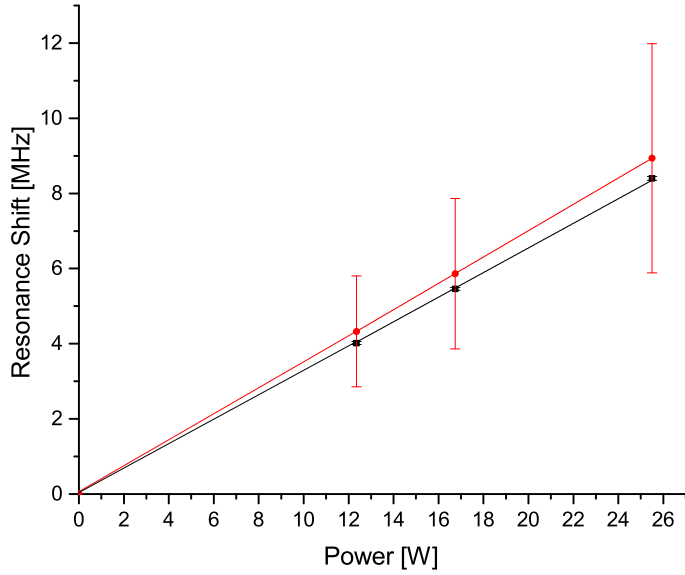


Figure 5.2.: Comparison of the differential light-shift in theory (red) and experiment (black) for the D₂-line. Note, that the scales show the initial laser powers. The power in the middle of the trap itself is twice as strong. As is visible in this plot, the errors for the measured shifts are very small compared to that of the calculated value. This supports the assumption, that the error is mostly systematic and can be removed in comparison with the measured results.

power, that we know with good precision.

$$I = \frac{\epsilon_0 c}{\alpha} \cdot U \quad (45)$$

$$w_0 = \sqrt{\frac{2P}{\pi I}} \quad (46)$$

In this calculation I is the actual maximum-intensity forming the potential and P the initial laser-power in the trap. For the crossed dipole-trap this results in the following waist.

$$w_0 = 41.383 \pm 0.082 \mu\text{m} \quad (47)$$

The approximate value used for the calculation, taken from [15] was $40 \mu\text{m}$.

5. Measurement in the dipole trap

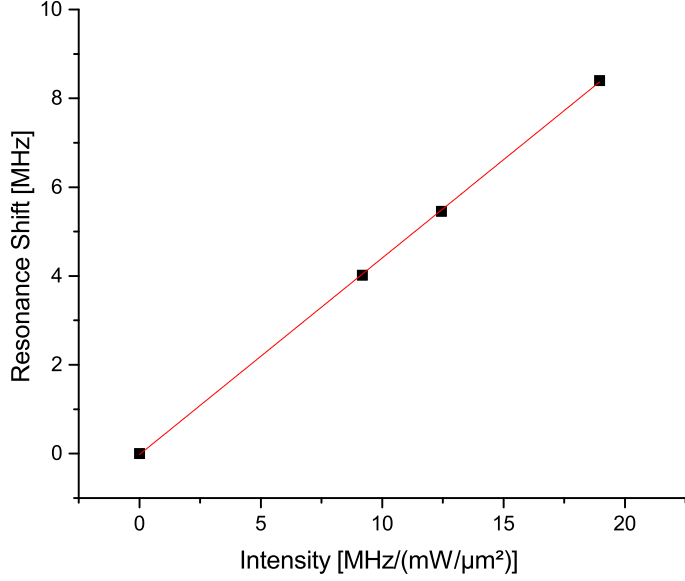


Figure 5.3.: Measured differential shift in terms of intensity.

5.1. MICROTRAP PARAMETERS

Using the tested theory we now can calculate the depth for the microtrap. The current waist of the trap is $1.3 \mu\text{m}$ using laser power of $400 \mu\text{W}$. This leads to a trap depth of

$$U_g = -(6.03 \pm 0.61) \mu\text{K} k_B \quad (48)$$

$$U_e = -(3.90 \pm 0.39) \mu\text{K} k_B \quad (49)$$

Assuming a 5%-error on the beams waist. We can use $p_\gamma = h/\lambda$ and $T_{Li} = p^2/2m_{Li}$ to calculate recoil energy excited Lithium-6 atom. The trap depth corresponds roughly to the recoil of only a single photon. Therefore the trap is not deep enough for holding an atom for enough absorption events to actually measure the fluorescence. However, it is possible in our setup to ramp the laser power up to about 500 mW, that would correspond to about 1400 photon recoil energies.

$$U_g = -(7.54 \pm 0.76) \text{ mK} k_B \quad (50)$$

$$U_e = -(4.88 \pm 0.49) \text{ mK} k_B \quad (51)$$

Taking this as an upper limit in scattered photons before escaping the potential it seems possible to catch enough light of the atoms to detect their fluorescence on the camera.

6. CONCLUSION AND OUTLOOK

The goal of this thesis was to determine the AC-Stark shift in order to evaluate the possibilities of spatially resolved imaging of single atoms in our microtrap setup. It was calculated and measured in the experiment using our crossed dipole trap. The experimental values proved to be in good consistency with the underlying theory. A summary of the results:

For the Lithium-6 ground and excited states ($2s_{1/2}$ and $2p_{3/2}$) the potential of a red detuned dipole trap is attractive. The resulting force however is weaker for the excited state. Compared to the ground state, at the used wavelength of 1064 nm, the potential depth for the excited state is about as 77 % for $|m_J| = 1/2$ and 65 % for $|m_J| = 3/2$ respectively. Inside the microtrap potential this results in a depth of 1 up to 1400 photon recoil energies, depending on the power of the trap beams. Since the kinetic energy directly links to the number of the scattered photons, this also gives a number, how much light can be absorbed and re-emitted, before the atoms are hot enough to escape the trap's boundaries. In contrast to other used imaging techniques with longer exposure times, capturing this low amount of light needs a more specialized optical system with higher performance.

Our objective, that is used to catch the fluorescence emission has a high numerical aperture and 10 % solid angle coverage. The used EMCCD camera (Andor iXon Ultra 897) allows single photon sensitivity. To get a discernible signal we estimate that we should capture at least 10 photons per atom, which would correspond to 100 scattering events. Considering the maximum depth of the trap, site-resolved imaging of single atoms should therefore be possible.

The next step would be to expand the current double well system. Trap stabilization and additional wells would enable new experiments. The first goal would be implementing four individual sites. These could be either arranged in a row or square, being the first block of a 2D optical lattice, but with full control over each individual lattice site. It would be possible to study long-ranged correlations in a linear chain, as well as to analyze the occurrence of many body effects, adding new lattice sites, one by one (see also [27]).

A. APPENDIX

A.1. POTENTIAL OF AN INDUCED DIPOLE MOMENT

The force on a dipole is given by [28]:

$$\mathbf{F} = (\mathbf{p} \cdot \nabla) \mathbf{E} \quad (52)$$

We know that the following holds:

$$\nabla(\mathbf{p} \cdot \mathbf{E}) = \mathbf{p} \times (\nabla \times \mathbf{E}) + \mathbf{E} \times (\nabla \times \mathbf{p}) + (\mathbf{p} \cdot \nabla) \mathbf{E} + (\mathbf{E} \cdot \nabla) \mathbf{p} \quad (53)$$

We consider the trap to consist of a retro-reflected laser beam, that is in phase, so the B-field-component of the electromagnetic wave is considered to be 0 as well as $\nabla \times \mathbf{E} = -\partial \mathbf{B} / \partial t = 0$. In our case the dipole-moment is not constant but $\mathbf{p} = \alpha \mathbf{E}$ and thus becomes:

$$\nabla(\mathbf{p} \cdot \mathbf{E}) = \alpha \mathbf{E} \times (\nabla \times \mathbf{E}) + \alpha \mathbf{E} \times (\nabla \times \mathbf{E}) + (\alpha \mathbf{E} \cdot \nabla) \mathbf{E} + \alpha (\mathbf{E} \cdot \nabla) \mathbf{E} \quad (54)$$

which becomes:

$$\begin{aligned} \nabla(\mathbf{p} \cdot \mathbf{E}) &= 2\alpha(\mathbf{E} \cdot \nabla) \mathbf{E} = 2(\mathbf{p} \cdot \nabla) \mathbf{E} \\ \Rightarrow \mathbf{F} &= \frac{1}{2} \nabla(\mathbf{p} \cdot \mathbf{E}) \end{aligned}$$

To get the corresponding potential one has to integrate the force. For a rapidly oscillating field we further have to take the time average to get an effective value for the trapping potential.

$$U = -\frac{1}{2} \langle \mathbf{p} \cdot \mathbf{E} \rangle \quad (55)$$

A.2. WIGNER 3-J AND 6-J SYMBOLS

The Wigner 3-j symbol and 6-j symbols are short notations, defined in terms of Clebsch-Gordan-Coefficients:

$$\begin{pmatrix} j_1 & j_2 & j_3 \\ m_1 & m_2 & m_3 \end{pmatrix} := \frac{(-1)^{j_1-j_2-m_3}}{\sqrt{2j_3+1}} \langle j_1 m_1 j_2 m_2 | j_3 - m_3 \rangle \quad (56)$$

$$\left\{ \begin{matrix} j_1 & j_2 & j_3 \\ j_4 & j_5 & j_6 \end{matrix} \right\} := \sum_{m_j}^6 (-1)^{\sum_{k=1}^6 (j_k - m_k)} \begin{pmatrix} j_1 & j_2 & j_3 \\ m_1 & m_2 & -m_3 \end{pmatrix} \begin{pmatrix} j_1 & j_5 & j_6 \\ -m_1 & m_5 & m_6 \end{pmatrix} \quad (57)$$

$$\times \begin{pmatrix} j_4 & j_5 & j_3 \\ m_4 & -m_5 & m_3 \end{pmatrix} \begin{pmatrix} j_4 & j_2 & j_6 \\ -m_4 & -m_2 & -m_6 \end{pmatrix} \quad (58)$$

A. Appendix

A.3. WIGNER-ECKART THEOREM

The Wigner-Eckart theorem simplifies the calculation of matrix-elements in a spherical basis and breaks it down to the calculation of few reduced matrix elements. For an irreducible tensor-operator T_q^r between two angular-momentum eigenstates the following holds [29, p. 17]:

$$\langle j, m_j | T_q^r | k, m_k \rangle = \langle j || T^r || k \rangle C_{rkm_k}^{jm_j} \quad (59)$$

In this formula r denotes the rank of the tensor, and q is simply the respective component of the tensor. Writing this in terms of the 3-j symbols yields:

$$\langle j, m_j | T_q^r | k, m_k \rangle = (-1)^{j-m_j} \begin{pmatrix} j & r & k \\ -m_j & q & m_k \end{pmatrix} \langle j || T^r || k \rangle \quad (60)$$

The resulting reduced matrix elements are independent of the respective component of the operator and the m -quantum-number. Therefore for every pair of angular-momentum quantum numbers j and k only one reduced matrix element has to be calculated to evaluate all elements of eigenstates involving said angular momenta.

BIBLIOGRAPHY

- ¹P. W. Anderson, “The resonating valence bond state in $\text{La}_2\text{Cu}_3\text{O}_4$ and superconductivity”, *Science* **235** (1987).
- ²R. Feynman, “Simulating physics with computers”, *International Journal of Theoretical Physics* **21** (1982).
- ³H. J. Metcalf and P. V. der Straten, *Laser cooling and trapping* (1999).
- ⁴I. Bloch, J. Dalibard, and S. Nascimbene, “Quantum simulations with ultracold quantum gases”, *Nature Physics* **8** (2012).
- ⁵M. Greiner, “Ultracold quantum gases in three-dimensional optical lattice potentials”, PhD thesis (Ludwig-Maximilians-Universität München, 2003).
- ⁶W. Ketterle, D. Durfee, and D. Stamper-Kurn, “Making, probing and understanding bose-einstein condensates”, (1999).
- ⁷W. S. Bakr, J. I. Gillen, A. Peng, S. Fölling, and M. Greiner, “A quantum gas microscope for detecting single atoms in a hubbard-regime optical lattice”, *Nature* **462** (2009).
- ⁸J. F. Sherson, C. Weitenberg, M. Enders, M. Cheneau, I. Bloch, and S. Kuhr, “Single-atom-resolved fluorescence imaging of an atomic mott insulator”, *Nature* **467** (2010).
- ⁹P. M. Preiss, R. Ma, E. Tai, J. Simon, and M. Greiner, “Quantum gas microscopy with spin, atom-number, and multilayer readout”, *Physical Review Letters* **91** (2015).
- ¹⁰E. Haller, J. Hudson, A. Kelly, D. A. Cotta, B. Peaudecerf, G. D. Bruce, and S. Kuhr, “Single-atom imaging of fermions in a quantum-gas microscope”, (2015).
- ¹¹S. Murmann, A. Bergschneider, V. M. Klinkhamer, G. Zürn, and S. Jochim, “Two fermions in a double well: exploring a fundamental building block of the hubbard model”, *Physical Review Letters* **114** (2015).
- ¹²R. Bücker, A. Perrin, S. Manz, T. Betz, C. Koller, T. Plisson, J. Rottmann, T. Schumm, and J. Schmiedmayer, “Single-particle-sensitive imaging of freely propagating ultracold atoms”, *New Journal of Physics* **11** (2009).
- ¹³A. J. Hillard, Y. H. Fung, P. Sompet, A. V. Carpentier, and M. F. Andersen, “In-trap fluorescence detection of atoms in a microscopic dipole trap”, (2015).
- ¹⁴F. Serwane, “Deterministic preparation of a tunable few-fermion system”, PhD thesis (Universität Heidelberg, 2011).
- ¹⁵T. Lompe, “Efimov physics in a three-component fermi gas”, PhD thesis (Universität Heidelberg, 2011).
- ¹⁶F. Serwane, G. Zürn, T. Lompe, T. B. Ottenstein, A. Wenz, and S. Jochim, “Deterministic preparation of a tunable few-fermion system”, *Science* **332** (2011).

Bibliography

- ¹⁷Making, probing and understanding ultracold fermi gases, Proceedings of the International School of Physics "Enrico Fermi" (2008).
- ¹⁸T. B. Ottenstein, "Few-body physics in ultracold fermi gases", PhD thesis (Universität Heidelberg, 2010).
- ¹⁹M. E. Gehm, "Preparation of an optically-trapped degenerate fermi gas of ⁶Li: finding the route to degeneracy", PhD thesis (Duke University, 2003).
- ²⁰W. Demtröder, *Experimentalphysik 3*, 4th ed. (2010).
- ²¹U. Freiburg, (May 11, 2015) http://ruby.chemie.uni-freiburg.de/Vorlesung/SVG/Methoden_ac/li_spektrum_svg.svg.
- ²²R. Grimm, M. Weidemueller, and Y. B. Ovchinnikov, "Optical dipole traps for neutral atoms", (1999).
- ²³W. R. Johnson, "Scalar and tensor polarizabilities of atoms", (2009).
- ²⁴M. S. Safronova, U. I. Safronova, and C. W. Clark, "Magic wavelengths for optical cooling and trapping of lithium", (2012).
- ²⁵A. Kramida, Yu. Ralchenko, J. Reader, and NIST ASD Team, NIST Atomic Spectra Database (ver. 5.2), [Online]. Available: <http://physics.nist.gov/asd> [2015, May 11]. National Institute of Standards and Technology, Gaithersburg, MD. 2014.
- ²⁶C. Cohen-Tannoudji, J. Dupont-Roc, and G. Grynberg, *Atom-photon interactions* (1998).
- ²⁷S. Trebst, U. Schollwoeck, M. Troyer, and P. Zoller, "D-wave resonating valence bond states of fermionic atoms in optical lattices", Physical Review Letters **96** (2006).
- ²⁸T. Pudlik, (May 8, 2015) <http://physics.stackexchange.com/questions/38343/why-is-there-a-factor-of-1-2-in-the-interaction-energy-of-an-induced-dipole-with>.
- ²⁹W. R. Johnson, *Lectures on atomic physics* (2006).

ERKLÄRUNG

Ich versichere, dass ich diese Arbeit selbstständig verfasst und keine anderen als die angegebenen Quellen und Hilfsmittel benutzt habe.

Heidelberg, den 26.05.2015,